

AD-A148 673

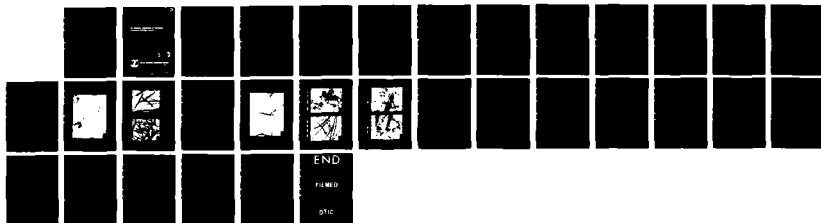
PHYSICAL PROPERTIES OF THE NICKEL COMPOSITE SINTERED
PLAQUE(U) NAVAL SURFACE WEAPONS CENTER SILVER SPRING MD
W A FERRANDO ET AL. DEC 82 NSWC/TR-82-416

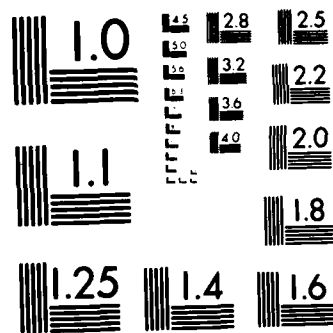
1/1

UNCLASSIFIED

F/G 10/3

NL





MICROCOPY RESOLUTION TEST CHART
NATIONAL BUREAU OF STANDARDS 1963-A

NSWC TR 82-418

AD-A148 673

THE PHYSICAL PROPERTIES OF THE BOND COMPOSITE SINTERED PLANNING

BY W. A. FERRANDO W. W. LEE A. L. LEE R. J. BROWN

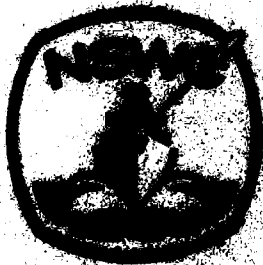
RESEARCH AND TECHNOLOGY DEPARTMENT

DECEMBER 1982

Approved for public release; distribution unlimited

DTIC
S E D
DEC 75 1982
E

DTIC FILE COPY



NAVAL SURFACE WEAPONS CENTER

Dahlgren, Virginia 22448 • Silver Spring, Maryland 20910

84 12 12 000

UNCLASSIFIED

SECURITY CLASSIFICATION OF THIS PAGE (When Data Entered)

20. (Cont.)

Porosities of 55 to over 90 percent void volume are achievable with the composite plaques, while maintaining structural integrity. Porosimetry measurements indicate approximately a 4X greater than mean pore size and 1.5X broader pore size distribution than commercial powder sinter. Tensile strengths were measured as a function of nickel coating thicknesses. A strength of 75-85kg/cm² was observed for plaques with fiber nickel coating thickness of about 1μ. Electrical resistivities of 400-600μ·Ω·cm were measured for plaques 1.0mm thick fabricated from fibers with 0.6-1.0μ thick nickel coating.

UNCLASSIFIED

SECURITY CLASSIFICATION OF THIS PAGE (When Data Entered)

FOREWORD

This report explores some of the important physical parameters of the fiber composite nickel plaque under development at NSWC. Results from electrical resistivity, tensile strength, porosity by standard measurement techniques and plaque structure provided by scanning electron micrography have shown that lightweight, durable, and energy efficient electrodes can be fabricated.

Comparison with a high quality commercial nickel sintered plaque shows acceptable performance of the composite in every area. Moreover, a considerable range of overlap with parameter values common in powder sinters exists for the composite. This allows an excellent opportunity to optimize the latter for specific requirements. In addition to being lightweight, the composite plaques possess the desirable feature of a highly open, interconnected structure which is easily impregnated with active material.

The authors express their appreciation to Dr. M. K. Norr of the center for his fine work in providing the SEM photographs.

Approved by:

J. R. Dixon
JACK R. DIXON, Head
Materials Division

Accession For	
SEARCHED	<input checked="" type="checkbox"/>
SERIALIZED	<input type="checkbox"/>
INDEXED	<input type="checkbox"/>

A-1

CONTENTS

	<u>Page</u>
INTRODUCTION	1
EXPERIMENTAL PROCEDURE	1
POROSITY	2
PLAQUE PORE SPECTRUM BY MERCURY INTRUSION POROSIMETRY	2
SCANNING ELECTRON MICROSCOPIC STUDY	7
SINTER BOND STRENGTH	7
PLAQUE DURABILITY	7
PLAQUE MORPHOLOGY	10
ELECTRICAL RESISTIVITY	14
TENSILE STRENGTH	17
CONCLUSIONS	17

ILLUSTRATIONS

<u>Figure</u>		<u>Page</u>
1	PLAQUE POROSITY VERSUS NICKEL COATING THICKNESS AT CONSTANT FIBER CONTENT	5
2	PLAQUE PORE SPECTRUM BY MERCURY INTRUSION POROSIMETRY	6
3	SEM PHOTOGRAPH OF FRACTURED SINTER BOND	8
4	SEM PHOTOGRAPH OF COMPOSITE PLAQUE "CYCLED" 1000X	9
5	CORROSION RESISTANCE OF COMPOSITE PLAQUE IN ELECTROLYTE	11
6	MORPHOLOGY, PORE SIZE COMPARISON COMPOSITE VERSUS POWDER SINTER	12
7	IMPREGNATED COMPOSITE PLAQUE DISTRIBUTION OF ACTIVE MATERIAL	13
8	ELECTRICAL RESISTIVITY VERSUS COMPACTION PRESSURE	15
9	ELECTRICAL RESISTIVITY VERSUS NICKEL COATING THICKNESS.	16
10	TENSILE STRENGTH VERSUS COMPACTION PRESSURE	18
11	TENSILE STRENGTH VERSUS NICKEL COATING THICKNESS.	19

TABLES

<u>Table</u>		<u>Page</u>
1	COMPOSITE PLAQUE PARAMETERS	3

INTRODUCTION

A new concept in sintered plaque fabrication for use in electrode production for nickel alkaline battery systems is the nickel composite plaque.¹ This plaque is made from highly graphitized carbon pitch mat fibers, coated with electroless nickel, compressed around a grid and sintered in a reducing (H₂) atmosphere. The result is a strong lightweight sintered composite structure of open porosity suitable for use in various battery electrodes.

This report discusses the physical properties of this composite plaque material. These results have been derived from tests on only two sets of plaques and, therefore, must not be considered exhaustive. The reported data establishes an acceptable baseline for the composite plaque which can be compared to that of powder sintered plaques. The four test areas include tensile strength, porosity, resistivity and SEM micrography of the plaque structure.

EXPERIMENTAL PROCEDURE

Sintered nickel plaques have been the substrate of choice for many years as a medium for incorporation of electrochemically active material in secondary alkaline battery systems, where high rate capability and durability are important. Such plaques have been made conventionally by sintering a fine nickel powder.² They have the advantage of providing a highly conductive and porous substrate for containing the active species. Their disadvantages include weight and material/fabrication costs. The nickel composite plaque addresses these factors. The composite plaque is made by coating a graphite fiber mat (Thornel Type "P" VMA Grade, Union Carbide Corp.) using an electroless nickel solution (Allied-Kelite, Richardson Chemical Company). The nickel coated fiber is placed under compaction pressure around a current collection grid and sintered in a reducing (H₂) atmosphere.

All composite plaques used in this study were made from available graphite mat containing fibers approximately 7-17 μ in diameter (1 μ = 10⁻⁶ meter).

The electroless nickel coating, containing 2 to 10 percent phosphorous, has a eutectic point near 840°C. Sintering, therefore, must be carried out below this temperature to prevent the eutectic liquid from forming and running off the fibers during the process. A 2 hour sintering time is used, although based upon experience with powder sinters,² a period of 15 to 20 minutes is probably sufficient.

An initial set of plaques was sintered at 762°C and 812°C as a function of compaction pressure to assess the integrity of the fiber sinter bonds. A second set of plaques, containing the same amount of graphite fiber, was sintered as a function of nickel coating thickness to determine the effect of the nickel coating on the physical properties of the plaque. Typical data on the second plaque set is given in Table 1. This consisted of plaques produced with (nominal) nickel coating thicknesses of 0.3 to 1.5 μ and plaque thicknesses of .75, 1.0, and 2.5mm, containing pure nickel expanded mesh current collectors. For comparison, a series of 1.0mm thick plaques, made without the current collector grid, is included. Finally, a 0.70mm thick commercial sinter was measured for reference.

POROSITY

Porosity measurements were made by water imbibition. Figure 1 shows the dependence of porosity on nickel coating thickness for the 0.75 and 1.0mm plaques at constant fiber content of 2.1 and 2.6 grams respectively. A variation of about 15 percent is observed in porosity as a function of nickel coating thickness.

Porosities of 55 percent to 95 percent have been produced in the composite plaques by varying the degree of compaction pressure (plaque thickness) for a given fiber content prior to sintering. Plaques fabricated with nickel coatings less than 0.5 μ thick tend toward structural weakness, blistering and fiber separation. These problems, however, are caused by inadequately coated portions of fiber resulting from non-uniformity due to hand processing. Composite plaques of good quality were obtained with nickel coating thicknesses in the range of 0.6 to 0.9 μ .

PLAQUE PORE SPECTRUM BY MERCURY INTRUSION POROSIMETRY

The mercury intrusion porosimeter method produces data on the volume of mercury forced into a porous sample as a function of applied pressure. By computing the appropriate derivative $\Delta V_{Hg}/\Delta P$, the fractional porosity versus effective pore diameter is obtained. Figures 2(a) and 2(b) show the results of such measurements on a powder sinter and composite plaque, respectively.

TABLE 1. COMPOSITE PLAQUE PARAMETERS

Plaque Thickness mm(nom.)	Coating Thickness μ (nom.)	Porosity %	Resist- ivity $\mu\Omega\text{cm}$	Tensile Strength kg/cm^2	Dry Weight grams	Mean Pore Diameter μ
0.75	0.3	88	673	36*	5.9	-
0.75	0.6	81	545	62*	7.8	-
0.75	0.9	75	434	72*	10.9	-
0.75	1.5	73	348	69*	13.9	-
1.0	0.3	95	869	3.5	6.4	-
1.0	0.6	86	650	48*	8.1	-
1.0	0.9	79	517	50*	11.0	-
1.0	1.5	79	430	69*	13.7	-
1.0 w/o grid	0.3	94	4228	12	3.6	66.0

* Average of two runs
 ** Manufacturer spec
 † Crack observed in sinter
 ▽ Grid break

TABLE 1. (Cont.)

Plaque Thickness mm(nom.)	Coating Thickness μ (nom.)	Porosity %	Resist- ivity $\mu\Omega\text{cm}$	Tensile Strength kg/cm^2	Dry Weight grams	Mean Pore Diameter μ
1.0 w/o grid	0.6	83	1325	42	7.5	59.5
1.0 w/o grid	0.9	80	976	59	9.2	60.0
1.0 w/o grid	1.5	77	586	77	12.9	56.5
2.5	0.3	73	1578	19	13.7	-
2.5	0.6	80	1008	78	18.1	-
2.5	0.9	74	807	72	23.4	-
0.70 powder	-	84*	140	44† 121∇	14.1	15.0

* Average of two runs

** Manufacturer spec

† Crack observed in sinter

∇ Grid break

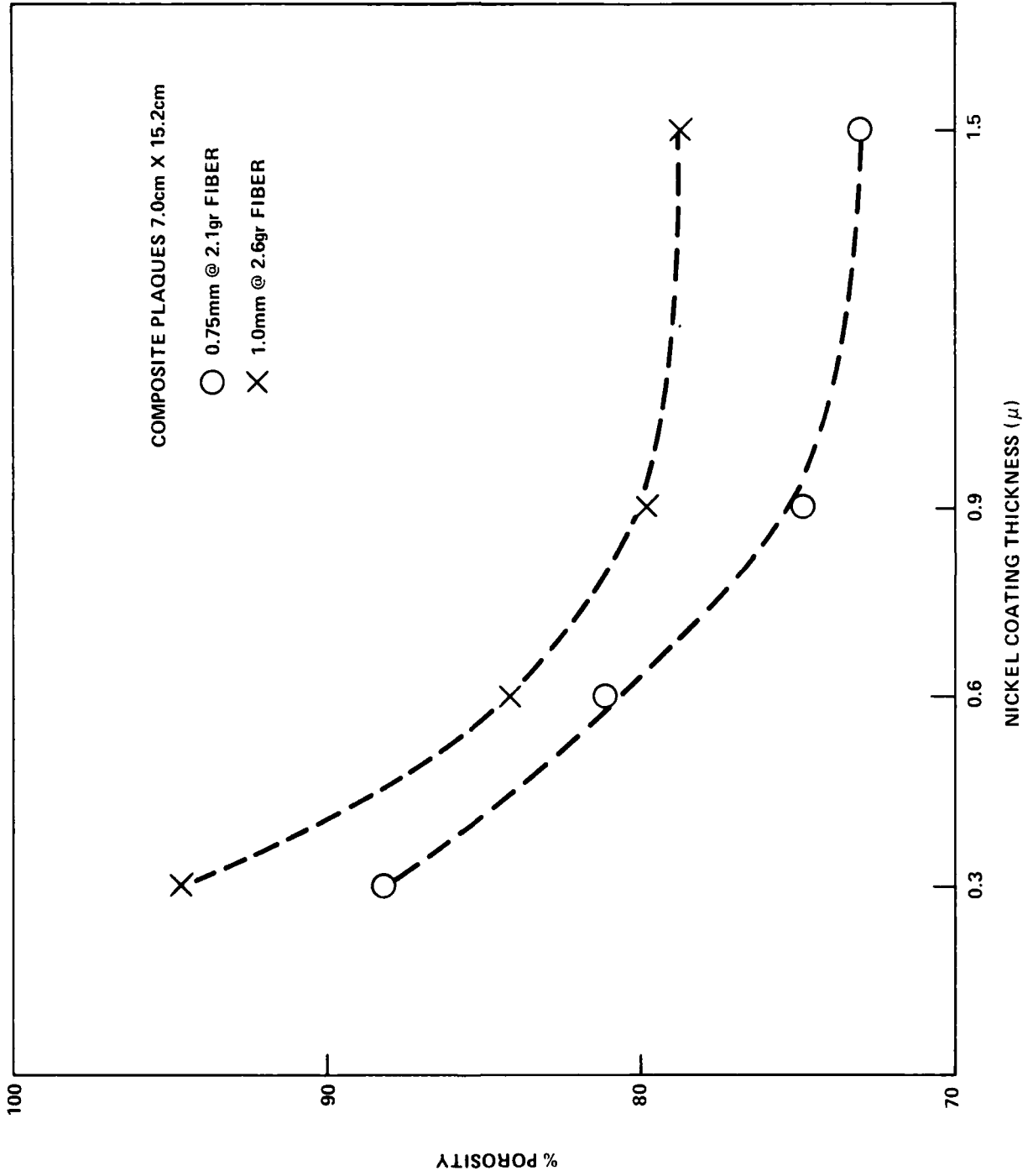
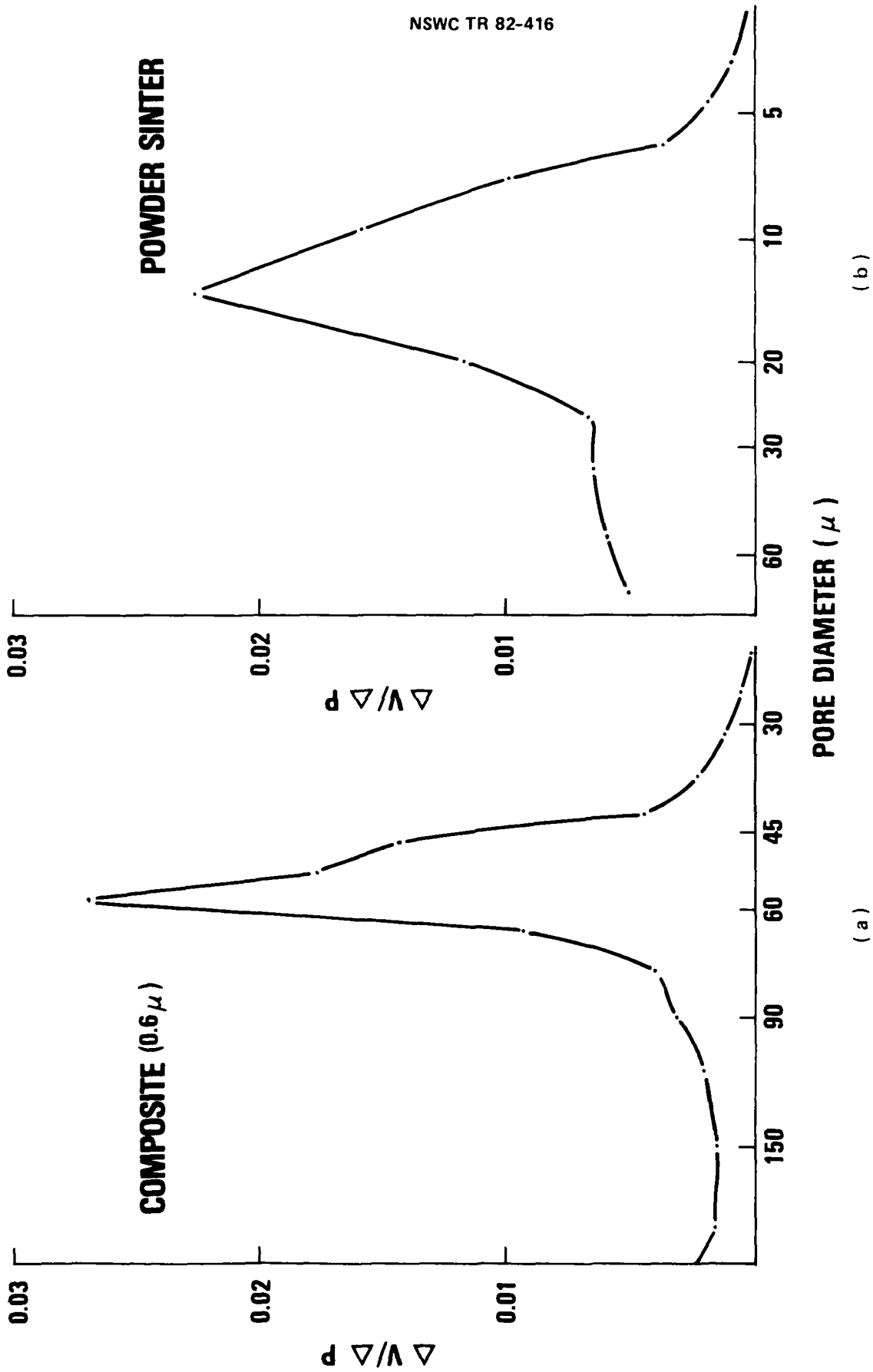


FIGURE 1. PLAQUE POROSITY VERSUS NICKEL COATING THICKNESS AT VARIOUS NICKEL COATING THICKNESSES AND FIBER CONTENT



(b)

(a)

FIGURE 2. PLAQUE PORE SPECTRUM BY MERCURY INTRUSION POROSIMETRY

The number of pores of effective diameter indicated along the log axis is proportional to the curve height. The figures have a roughly similar shape with the maximum void volume occurring at about 15μ for the powder sinter and 60μ for the composite plaque. The porosity distribution is about 50 percent broader in the latter. As the nickel coating thickness is varied from 0.3 to 1.5μ , the pore size distribution maximum shifts from 66μ to 56μ . These data quantify the pore size difference between the composite and typical powder plaque. For practical purposes the pores are considered spherical cavities. While this is far from the true topography of composite sinters, it is a convenient construct for cavity size comparisons.

The pore size versus nickel coating thickness dependence is not strong, as noted above. The 20 percent or so difference in pore size between plaques of thin and thick nickel coating is not likely to affect impregnation/formation conditions significantly. Of primary importance, however, is the 4X larger average pore size of the composite compared with powder sinters. The larger pores of the former may produce an electrode with some characteristics of the pocket plate. This implies some reduction in efficiency at high rate discharge compared with that of a powder sinter of equal thickness. Preliminary tests indicate that the composite plaque suffers a 5-10 percent penalty in active material utilization level compared with that typical of powder sinters. At this stage, the reduced utilization cannot be attributed reliably either to the larger pore size or marked differences in morphology between the composite and powder sinters. New, uniformly coated fibers of constant smaller diameter are becoming available. These will produce plaques of smaller, more uniform pore size, which will more closely match the pore size and surface area of the powder sinters.

SCANNING ELECTRON MICROSCOPIC STUDY

SINTER BOND STRENGTH

SEM photography is a powerful tool in examining sinter bonding, active material deposition, changes in morphology, etc. Figure 3 shows a portion of an impregnated plaque which has been cut and examined on edge. The stress of cutting has pulled apart two fibers at a sinter point, revealing the integrity of the sinter bond. This indicates the potential durability of the composite plaque under the physical and chemical stresses of cycling. The long-term plaque cycling test discussed below revealed that, although the nickel coating had considerably degraded, there was no evidence of disproportionate failure of the sinter bonds.

PLAQUE DURABILITY

Two tests of plaque durability were made. In the first, a portion of composite plaque was immersed in 31 percent KOH electrolyte at 75°C for 2 months with no applied potential. Figures 4(a) and 4(b) show this sample before and

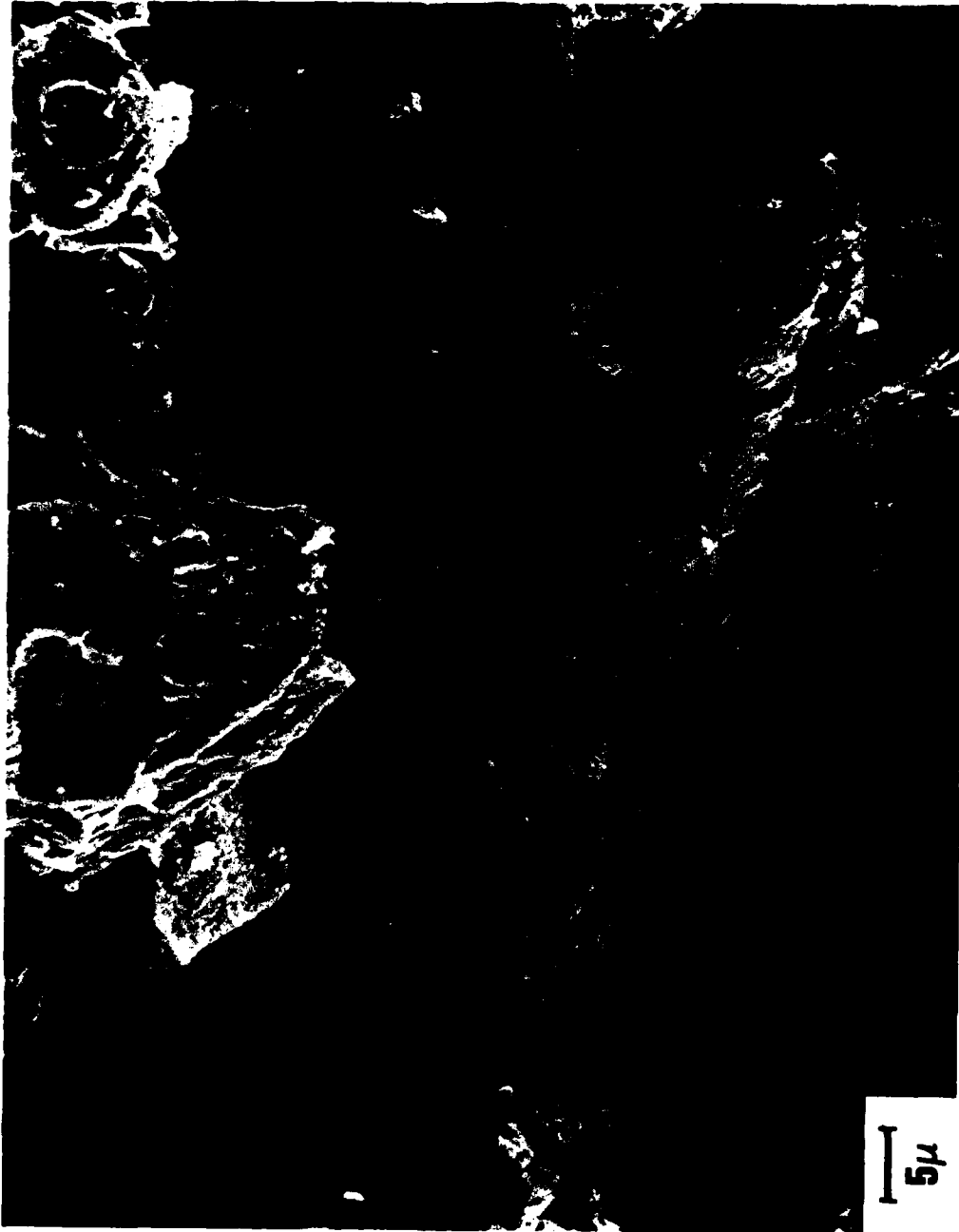


FIGURE 3. SEM PHOTOGRAPH OF FRACTURED SINTER BOND

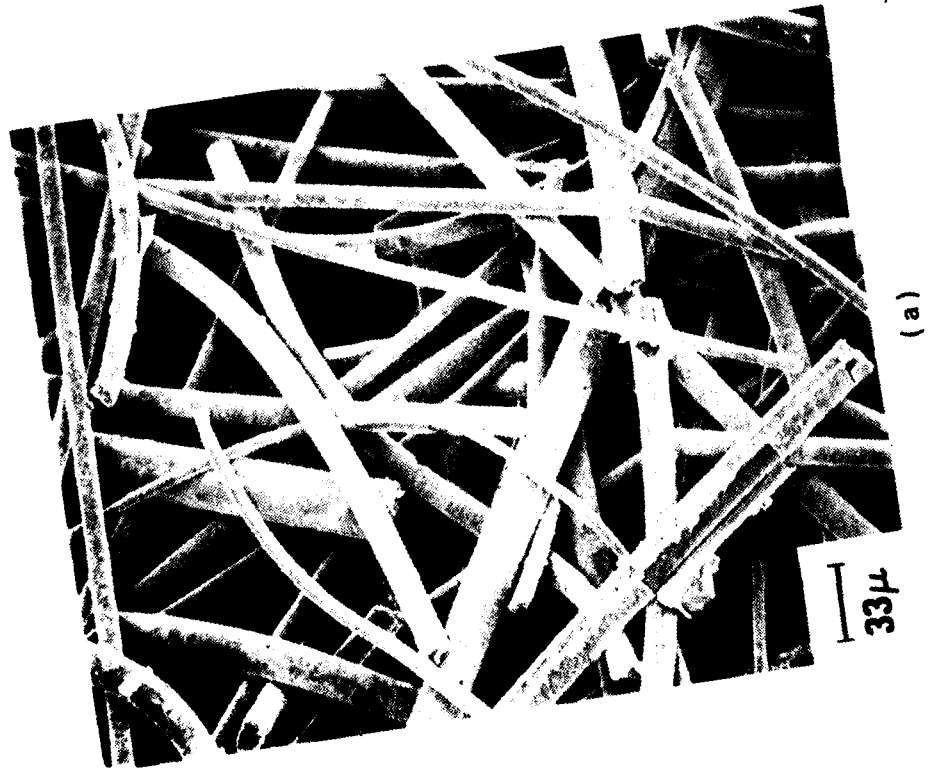
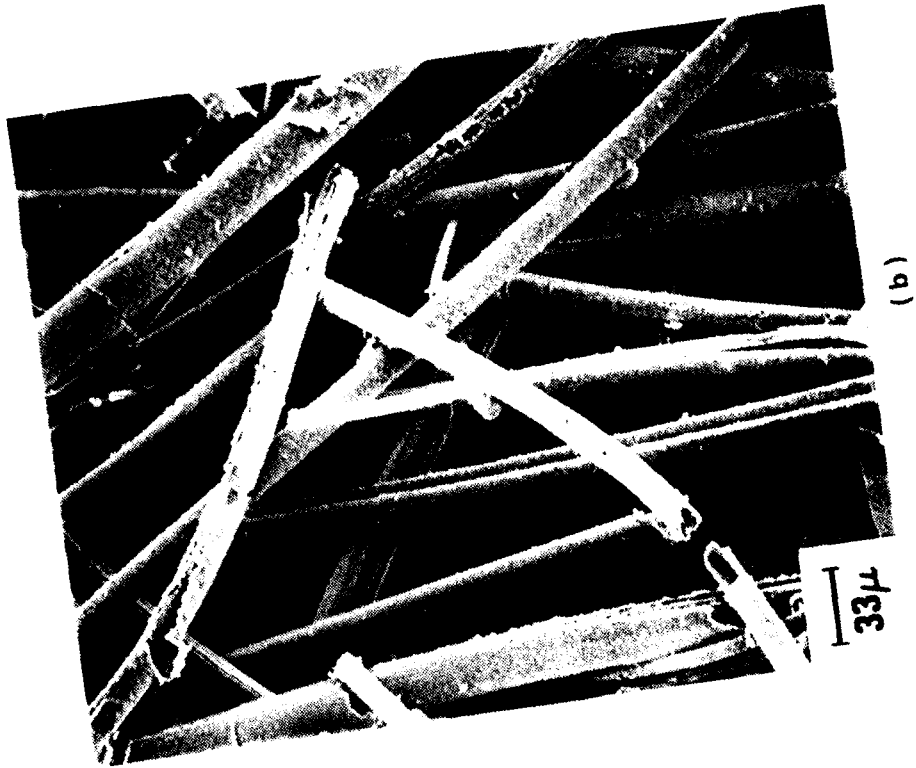


FIGURE 4. SEM PHOTOGRAPH OF COMPOSITE PLAQUE "CYCLED" 1000X

after immersion. No major corrosive attack is evident. Therefore, plaque deterioration does not occur under open circuit conditions in the electrolyte. This result implies a potentially long "shelf" life of the composite electrode.

The second test involved long term alternating anodization (charge) and cathodization (discharge) periods at moderate current density, equivalent to 1000 cycles. Figure 5 shows the plaque after this test. It remains intact although the surface has assumed an eroded appearance. Oxidation of the nickel coating produced the equivalent of about 7 percent the utilization of a fully impregnated electrode of similar dimensions. Some exposed and split fibers are evident, probably due to gradual electrolyte penetration. These oxidation and penetration processes will set the limit on composite plaque lifetime.

PLAQUE MORPHOLOGY

An estimate of pore size can be obtained from SEM photographs by measurement and comparison. Figures 6(a) and 6(b) show portions of composite plaque at 200X and powder sinter plaque at 1000X respectively. The contrast in morphology and pore size is evident. The composite is composed largely of wedge-shaped cavities arranged in an interconnected open structure. Sintering takes place at contact points of the randomly directed mat fibers. The powder sinter has generally smaller pore cavities. Sintering takes place along entire particle chains which aggregate to form cavities. A far greater number of sinter bonds are involved in forming the powder sinter plaque.

These SEM photographs do not give information on closed porosity. No systematic study in this area was attempted. Such an investigation will require several cross section photographs of an impregnated plaque to determine the presence of unimpregnated regions.

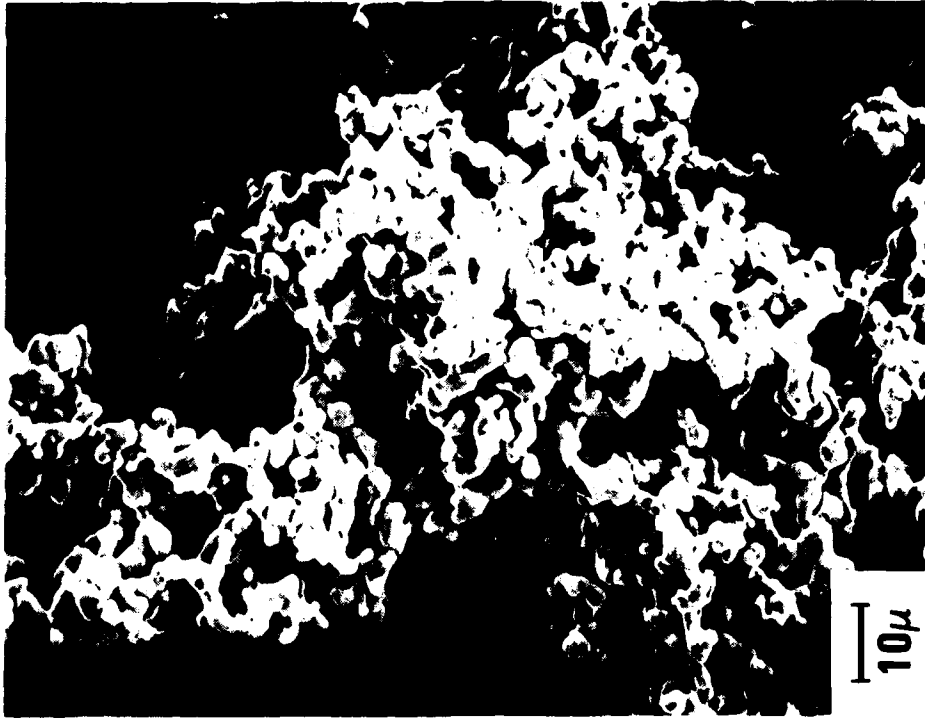
The mat fiber material used in the composite plaques has a specific surface area of $0.4\text{m}^2/\text{gram}$, compared with an area of 0.25 to $0.5\text{m}^2/\text{gram}$ for nickel powders after sintering. Therefore, due to a 2 to 2.5X greater mass/volume, powder sintered plaques have this factor advantage in pore surface area. Smaller surface area for a given porosity in the composite plaque implies larger average pore size.

Figures 7(a) and 7(b) show portions of the composite plaque after impregnation and after charge-discharge cycling, respectively. In Figure 7(a), the nickel composite electrode (Ni.C.E.) has been formed but not cycled. The active material (nickel hydroxide) is present as isolated lumps loosely bound within the pore cavities. After heavy cycling (>200) in a test cell, the active material has redistributed to conform to the cavity walls (Figure 7(b)). It has assumed a smooth, layered appearance with visible electrolyte flow channels. The active material apparently has optimized its electrical contact with the plaque. This is reflected in a marked increase (30 to 40 percent) in utilization between the initial and final states pictured in Figure 7. The sensitivity of electrode performance to plaque and active material morphology is aptly illustrated. Not only must the plaque have a large accessible pore surface area, but also the active material must be distributed to contact it intimately.



FIGURE 5. CORROSION RESISTANCE OF COMPOSITE PLAQUE IN ELECTROLYTE

1000X, POWDER SINTERED



(b)

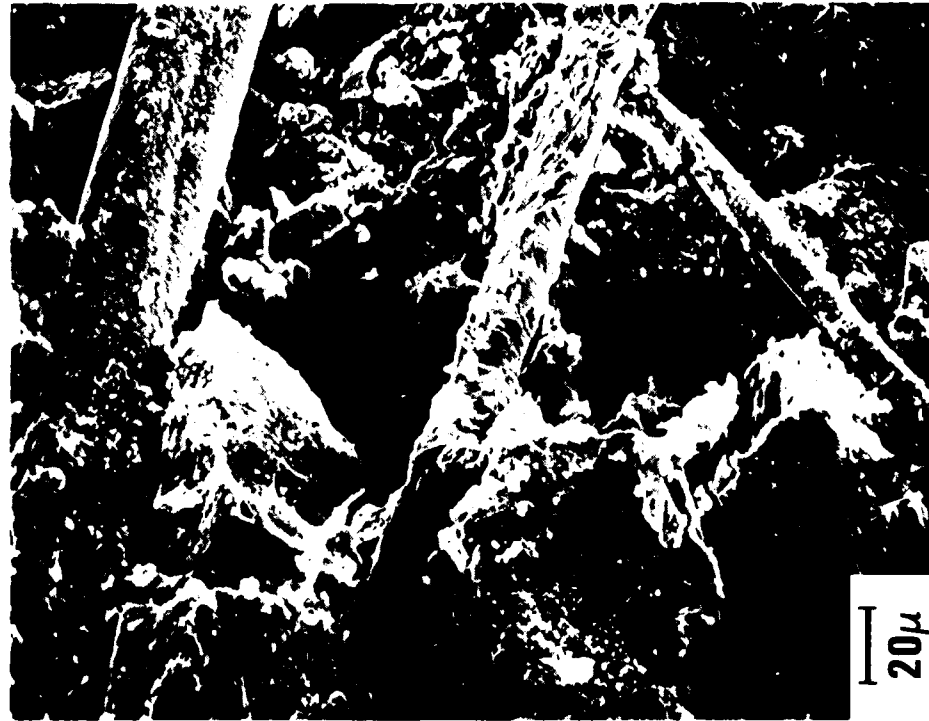
200X, FIBER SINTERED



(a)

FIGURE 6. MORPHOLOGY, PORE SIZE COMPARISON COMPOSITE VERSUS POWDER SINTER

500X UNCYCLED



(a)

500X CYCLED



(b)

FIGURE 7. IMPREGNATED COMPOSITE PLAQUE DISTRIBUTION OF ACTIVE MATERIAL

ELECTRICAL RESISTIVITY

For maximum utilization of the active material and electrical efficiency of a cell to be achieved, the electrode resistivity should be a minimum. Of concern in sintered plate battery systems is the plaque resistivity, which is an important contributor to the cell's internal resistance.

Electrical resistivities of the composite test plaques were measured using a four point probe method. A known current is passed through the plaque. A potential probe of fixed width is used to measure the voltage drop across a plaque segment. Using the thickness and other information, the local resistivity is computed. Such measurements were made on the series of composite plaques sintered at 762°C and 812°C. Figure 8 shows the electrical resistivity versus compaction pressure for this series. The cross-hatched region indicates the resistivity range common in nickel powder sinters. The best results were obtained at 812°C, 0.63 μ nickel coating.

Using this result as a baseline, a second set of plaques (Table 1) was fabricated and measured. Figure 9 displays the results of these measurements. Average plaque resistivity is plotted as a function of nickel coating thickness. Figure 9 shows that thin plaques have significantly lower resistivity than thick ones. For the same nickel coating thickness, a composite plaque 2.5mm thick has about twice the resistivity of one 0.75mm thick. The resistivity at each plaque thickness shows little decrease for coating thicknesses greater than about 0.6 μ . The relatively lower resistivity of the thin plaques can be accounted for by the increased volume fraction occupied by the current collector (a pure nickel 0.15mm thick expanded metal grid) in the thin plates. A series of 1.0mm thick plaques was produced without the current collector grid in order to assess its contribution. The results are plotted as the upper curve of Figure 9. In the absence of the current collector, for a given nickel coating thickness, 1.0mm thick plaque has about twice the resistivity.

For comparison, the isolated point at lower right in Figure 9 indicates the measured resistivity of a recently manufactured 0.70mm thick powder sintered plaque. Its resistivity of 140 $\mu\Omega\cdot\text{cm}$ is about one-third that of a typical 0.75 to 1.0mm composite plaque of this series. Intersection with the practical resistivity range (~ 200 to 750 $\mu\Omega\cdot\text{cm}$) determines the combinations of nickel coating and plaque thicknesses required for acceptable sinters. The data show that plaques thicker than 1.0mm will probably require heavier current collection grids to bring their resistivities within this range. If relatively thick nickel coatings are used, it might be possible to eliminate the current collector grid for some electrode applications.

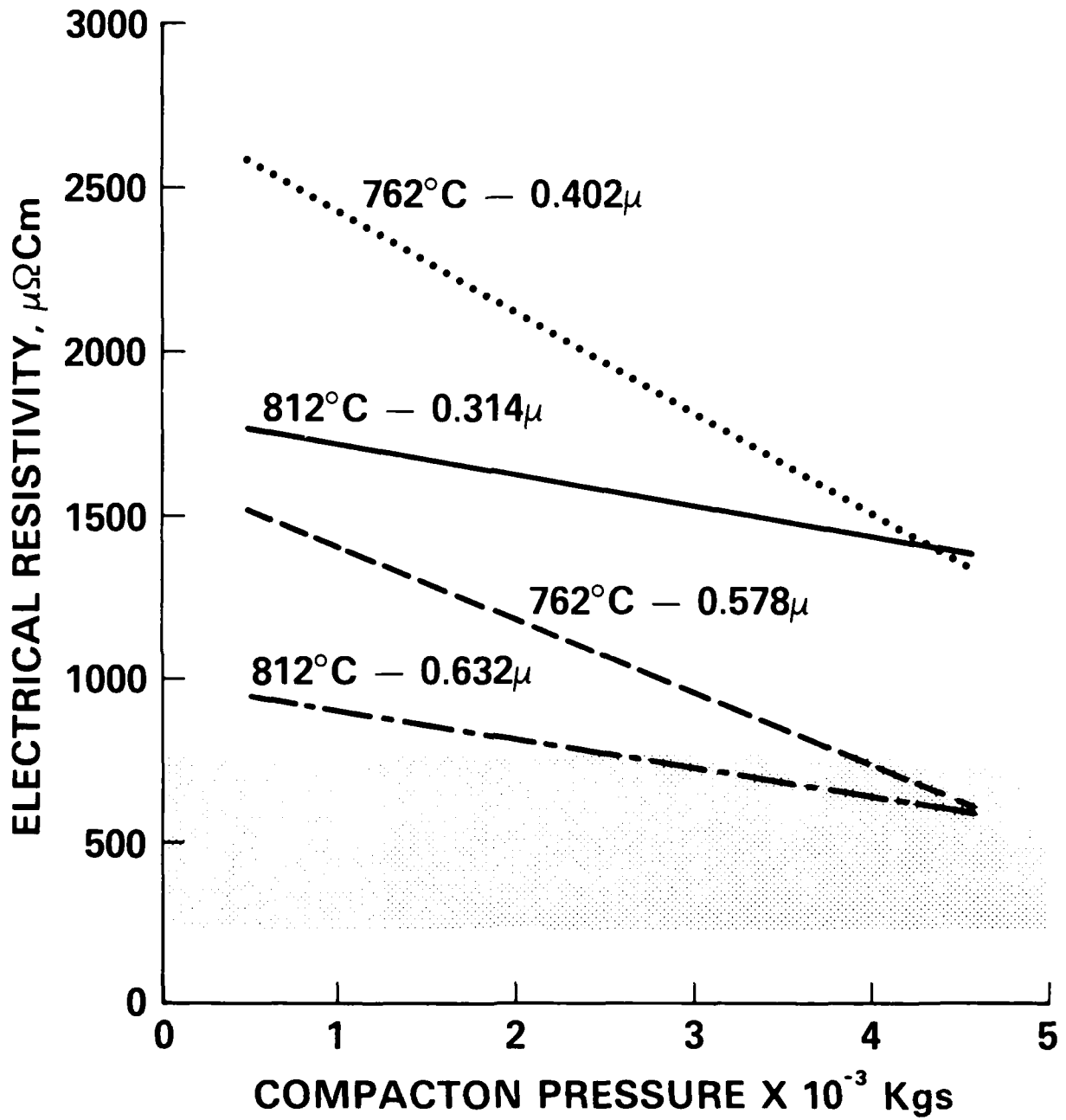


FIGURE 8. ELECTRICAL RESISTIVITY VERSUS COMPACTION PRESSURE

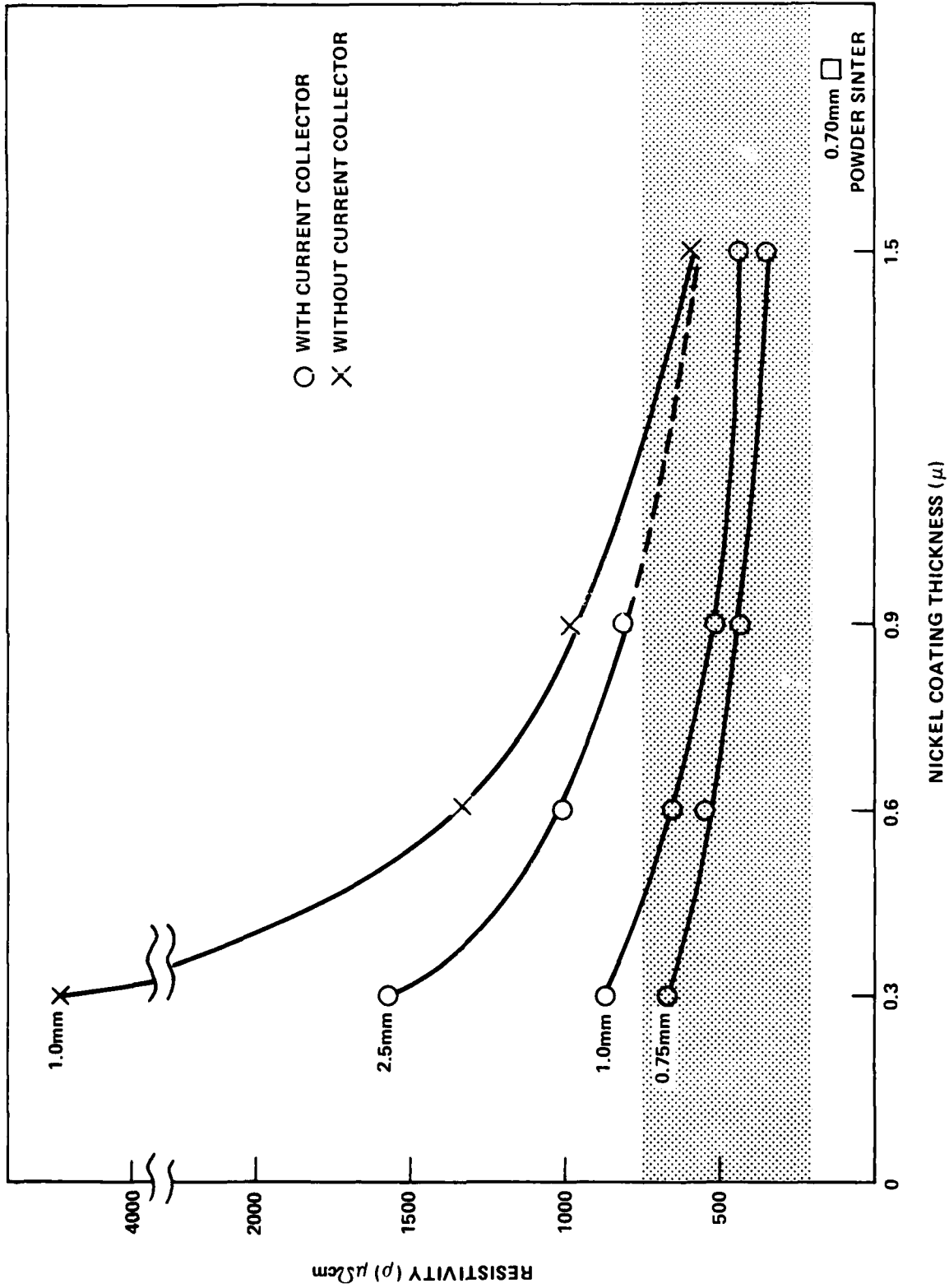


FIGURE 9. ELECTRICAL RESISTIVITY VERSUS NICKEL COATING THICKNESS

TENSILE STRENGTH

A simple test was used to determine the ultimate tensile strength of the composite plaques. The results were compared with those for powder sinters. The experimental arrangement used a hanging pedestal and weights to place the sample under static tension. The plaques were cut into strips of measured width. The only difficulty encountered was in devising a satisfactory holding method. Clamping the strip ends caused fiber damage and premature failure. The problem was solved by carefully epoxying small pieces of aluminum at each end of the strips. The test sample could then be placed conveniently under tension.

The load to failure (breakage) was recorded for each composite plaque sample of the first series. Figure 10 shows the failure load as a function of compaction pressure during sinter for various nickel coating thickness/temperature combinations. The cross-hatch area indicates the range of tensile strengths obtained in powder sinters under normal processing conditions. The composite sinters processed at 800°C with 0.6 μ nickel coating produced the best results.

A second set of composite sinters was tested. Failure strength as a function of nickel coating thickness is shown in Figure 11. Vertical bars indicate two measurements on the same plaque. The data show increasing strength up to a nickel coating thickness of about 0.9 μ . Above this coating thickness, the ultimate tensile appears to become constant at 75 kg/cm². By contrast, from the data of Figure 10, increasing fiber content with compaction pressure translates into linear increase in tensile strength over the measured range. These data also show that tensile strengths greater than 75kg/cm² are possible in the composite plaques by increasing their fiber content. However, a penalty will be paid in decreased porosity. The 0.70mm thick, recently manufactured, powder sinter plaque exhibited a crack in the sinter at about 45kg/cm² as indicated in Figure 11. The ultimate tensile strength of 110kg/cm² was due principally to its current collector grid strength rather than to the sinter body.

CONCLUSIONS

Porosity of the composite plaque may be varied over a wide range of 55 to >90 percent by altering its fiber content. The mean pore size of plaques subjected to testing was about 4X and width of distribution about 1.5X those of powder sinter plaques. The achievement of smaller pore size while maintaining high porosity in the composite plaques necessitates that a graphite material of somewhat smaller, more uniform fiber diameter be used.

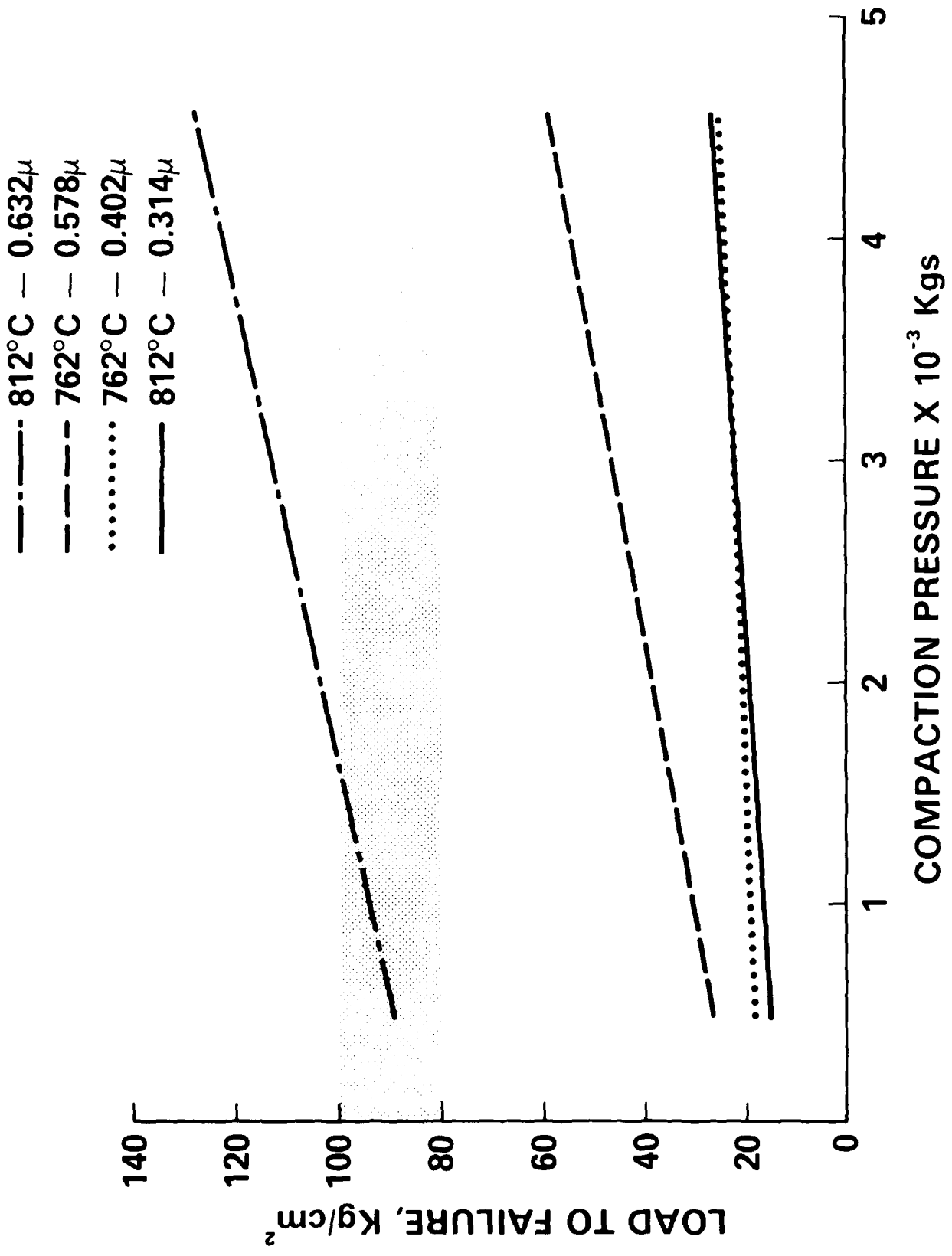


FIGURE 10. TENSILE STRENGTH VERSUS COMPACTION PRESSURE

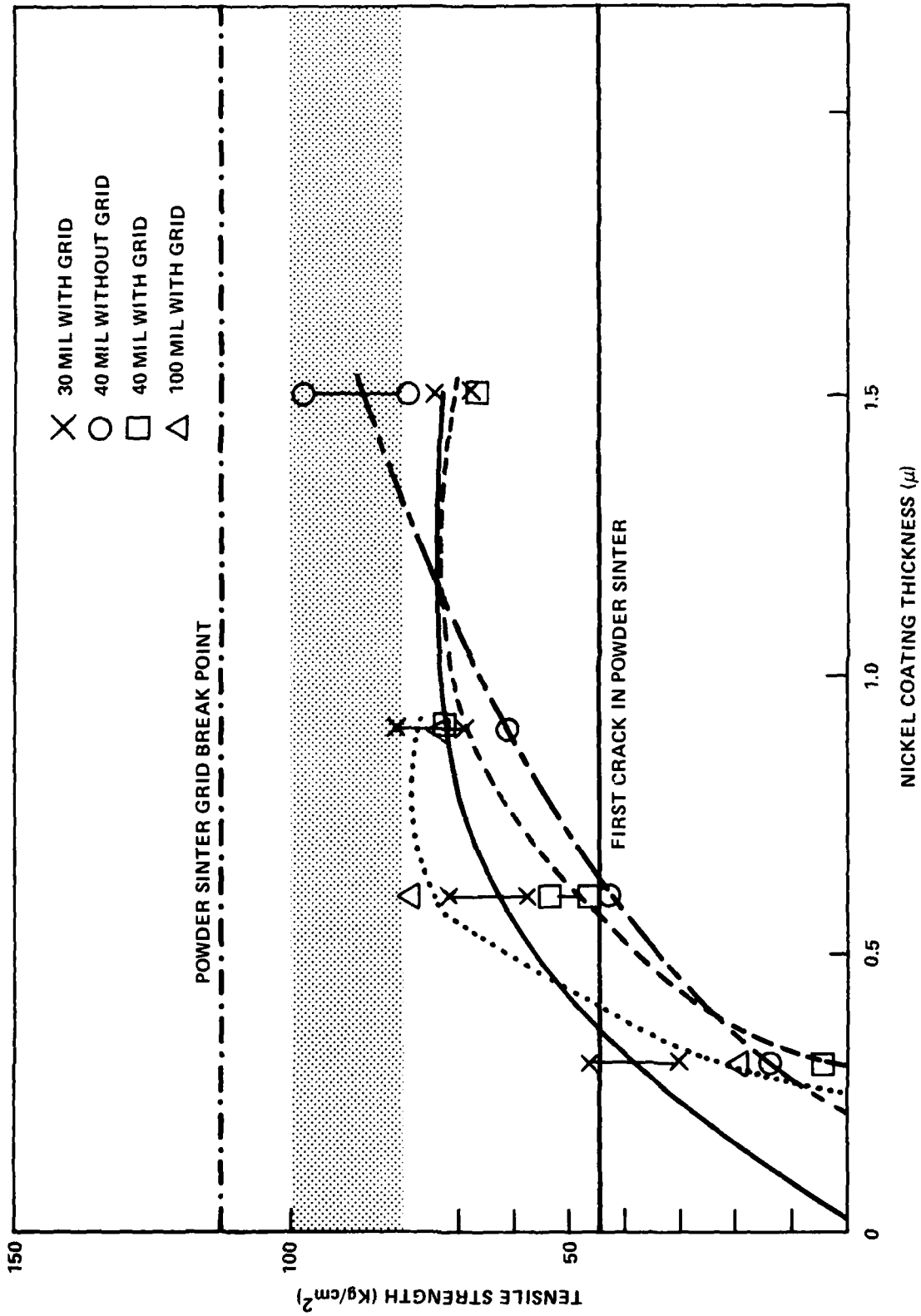


FIGURE 11. TENSILE STRENGTH VERSUS NICKEL COATING THICKNESS

SEM micrography confirms a composite plaque morphology of virtually 100 percent open interconnected porosity which readily accepts high active material impregnation levels. Micrographic observation of a cycled composite electrode indicates good intra-electrode electrolyte circulation.

The composite plaque electrical resistivity can be made comparable, by suitable nickel coating thickness, sinter temperature and fiber content, to that of typical powder sinters.

The ultimate tensile strength of the composite plaques increases with increasing nickel coating thickness, saturating at 75 to 85kg/cm² for nickel coating thicknesses around 0.9μ. The tensile load is carried by the composite fiber structure rather than by the nickel conductor grid.

Good durability was noted for the composite plaque against corrosion under long term immersion in hot KOH electrolyte. Stability against dissolution was demonstrated by the unimpregnated composite plaque under anodization (charge) with gas evolution and cathodization (discharge) conditions equivalent to 1000 cycles.

A sintering temperature of 800°C and nickel coating thickness of 0.6 to 0.9μ produce a composite plaque of suitable physical characteristics for cell use.

REFERENCES

1. Ferrando, W. A., and Sutula, R. A., "Lightweight Battery Electrode," U.S. Patent No. 4,215,190, 1980.
2. Falk, S. U., and Salkind, A. J., Alkaline Storage Batteries, (New York: John Wiley and Sons, Inc., 1969), p. 111.

DISTRIBUTION

	<u>Copies</u>		<u>Copies</u>
Defense Technical Information Center Cameron Station Alexandria, VA 22314	12	Office of Chief of Naval Operations Operation Evaluation Group Washington, DC 20350	1
Defense Nuclear Agency Attn: Library Washington, DC 20301	1	David W. Taylor Naval Ship Research and Development Center Attn: A. B. Neild (Code 2723) W. J. Levendahl (Code 2703) J. Woerner (Code 2724) H. R. Urbach (Code 2724) D. Icenhower (Code 2721) J. Gudas (Code 2813) W. Lukens (Code 2822)	1 1 1 1 1 1
Pentagon Project Officer, OSD(MRA&L)-WR Attn: William G. Miller Room 2B323 Washington, DC 20301	1	Annapolis Laboratory Annapolis, MD 21402	
Office of Deputy Under Secretary of Defense for Research and Engineering Staff Specialist for Materials and Structures Attn: Mr. Jerome Persh Room 3D1089, The Pentagon Washington, DC 20301	1	Naval Air Development Center Attn: Dr. E. McQuiller Dr. G. London Warminster, PA 18974	1 1
Defense Advanced Research Projects Agency Attn: E. Van Reuth L. Jacobsen 1400 Wilson Boulevard Arlington, VA 22209	1 1	Naval Air Systems Command Attn: Mr. R. Schmidt (Code 52031A) Washington, DC 20361	1
Institute for Defense Analyses R&E Support Division 400 Army-Navy Drive Arlington, VA 22202	1	Naval Electronic Systems Command Attn: A. H. Sobel (Code PME 124-31) Washington, DC 20360	1
Library of Congress Attn: Gift and Exchange Division Washington, DC 20540	4	Naval Intelligence Support Center Attn: Dr. H. Ruskie (Code 362) 4301 Suitland Road Washington, DC 20390	1

DISTRIBUTION (Cont.)

	<u>Copies</u>		<u>Copies</u>
Naval Material Command		Naval Underwater Systems Center	
Attn: Code 08T223	1	Attn: J. Moden (Code 36123)	1
J. Kelly (MAT 0725)	1	R. Lazar (Code 36301)	1
W. Holden (MAT 08E4)	1	Newport, RI 02841	
O. J. Remson (MAT 071)	1	Naval Weapons Center	
G. R. Spaulding (MAT 072)	1	Attn: A. Fletcher (Code 3852)	1
Washington, DC 20360		China Lake, CA 93555	
Naval Ocean Systems Center		Naval Weapons Support Center	
Attn: Code 922	1	Attn: M. Robertson	1
Dr. S. D. Yamomoto		Electrochemical Power Sources	
(Code 513)	1	Division	
P. D. Burke (Code 9322)	1	Crane, IN 47522	
San Diego, CA 92152		Office of Naval Research	
Naval Ordnance Station		Attn: G. Neece (Code 413)	1
Attn: Howard R. Paul	1	B. MacDonald (Code 471)	1
Project Manager		G. Sandoz (Code 715)	1
Southside Drive		J. Smith (Code 413)	1
Louisville, KY 40150		800 N. Quincy Street	
Naval Postgraduate School		Arlington, VA 22217	
Attn: Dr. William M. Tolles		Strategic Systems Project	
(Code 612)	1	Office	
Monterey, CA 93940		Crystal Mall No. 3	
Naval Research Laboratory		Attn: G. Needham (Code 273)	1
Attn: Dr. Fred Saalfeld		LCDR F. Ness (Code 234)	1
(Code 6100)	1	LCDR H. Nakayama	
A. Simon (Code 6130)	1	(Code 272)	1
S. C. Sanday (Code 6370)	1	Washington, DC 20362	
I. Wolock (Code 8433)	1	Army Electronics Research and	
H. Chaskelis (Code 8431)	1	Development Command	
4555 Overlook Avenue, S.W.		Attn: A. Legath (Code DELET-P)	2
Washington, DC 20375		S. Gilman	
Naval Sea Systems Command		(Code DRSEL-TL-P)	1
Attn: M. Kinna (Code 62R4)	1	E. Brooks	
J. DeCorpo	1	(Code DRSEL-TL-P)	1
E. J. Anderson	1	G. DiMasi	
Code 5433	1	(Code DRSEL-TL-P)	1
H. Vanderveldt		Fort Monmouth, NJ 07703	
(Code 05R15)	1	Army Foreign Science and	
Code 99612	2	Technology Center	
Code 0841B	1	Attn: J. F. Crider	
Washington, DC 20362		(Code FSTC/DRXST-MTI)	1
		220 7th Street	
		Charlottesville, VA 22901	

DISTRIBUTION (Cont.)

	<u>Copies</u>		<u>Copies</u>
Army Materials & Mechanics Research Center		Office of Chief of Research & Development	
Attn: J. J. DeMarco	1	Attn: Dr. S. J. Magram	1
J. W. McCauley	1	Department of the Army	
A. Levitt	1	Energy Conversion Branch	
J. Greenspan	1	Room 410, Highland Building	
F. Larson	1	Washington, DC 20315	
L. R. Aronin	1		
Watertown, MA 02172		Air Force Flight Dynamics Laboratory	
Army Material Development and Readiness Command		Attn: D. Roselius	1
Attn: J. W. Crellin		L. Kelley	1
(Code DRCDE-L)	1	Wright-Patterson Air Force Base	
5001 Eisenhower Avenue		Dayton, OH 45433	
Alexandria, VA 22333			
Army Mobility Equipment R&D Command		AF Weapons Laboratory	
Attn: J. Sullivan (Code DRXFB)	1	Attn: Charles Stein	1
G. D. Farmer, Jr.		Kirtland AFB	
(Code DRDME-VM)	1	Albuquerque, NM 87115	
Dr. J. R. Huff		Air Force Wright Aeronautical Laboratory	
(Code DRDME-EC)	1	Attn: M. Duhl (Code MB)	1
Electrochemical Division		T. Ronald (Code LLS)	1
Fort Belvoir, VA 22060		W. S. Bishop	
		(Code POOC-1)	1
Army Research Office		R. M. Neff	
Attn: B. F. Spielvogel	1	(Nonmetallic Mat. Div.)	1
J. C. Hurt	1	D. R. Beeler (Code MB)	1
P.O. Box 12211		D. Marsh	
Research Triangle Park, NC 27709		(Electrochemistry Code POOC-1)	1
Army Scientific Liaison & Advisory Group		Wright-Patterson AFB, OH 45433	
Attn: HQDA (DAEN-ASR-SL)	1	Frank J. Seiler Research Laboratory, AFSC	
Washington, DC 20314		Attn: LTCOL Lowell A. King	
Ballistic Missile Defense Officer		(Code FJSRL/NC)	1
BMD-ATC		USAF Academy, CO 80840	
Attn: M. L. Whitfield	1	SD/YLXT	
P.O. Box 1500		Attn: MAJ R. Gajewski	1
Huntsville, AL 35807		P.O. Box 92960, WPC	
		Los Angeles, CA 90009	

DISTRIBUTION (Cont.)

	<u>Copies</u>		<u>Copies</u>
Central Intelligence Agency		General Electric Company	
Attn: C. Sculla	1	Re-entry Systems Operations	
G. Methlie	1	Attn: K. J. Hall	1
Washington, DC 20505		P.O. Box 7722	
		Philadelphia, PA 19101	
Department of Energy		NASA Goodard Space Flight Center	
Attn: Dr. A. Landgrebe		Attn: G. Halpert (Code 711)	1
(Code MS E-463)	1	Greenbelt, MD 20771	
Division of Applied Technology			
Washington, DC 20545		NASA Headquarters	
Department of Energy		Attn: M. Greenfield (Code RTS-6)	1
Attn: L. J. Rogers (Code 2101)	1	Dr. J. H. Ambrus	1
Division of Electric Energy		600 Independence Avenue	
Systems		Washington, DC 20546	
Washington, DC 20545		NASA/Langley Research Center	
NASA Scientific and Technical		Attn: E. Mathauser (Code MS188A)	1
Information Facility		Dr. T. Bales	1
Attn: Library	1	Dr. D. Tenney	1
P.O. Box 33		Hampton, VA 23365	
College Park, MD 20740		Ms. A. L. Lee	
National Bureau of Standards		3004 Castleleigh Road	
Metallurgy Division		Silver Spring, MD 20904	1
Inorganic Materials Division	1	Internal Distribution:	
Washington, DC 20234		E431	9
NASA Lewis Research Center		E432	3
Attn: Mr. R. A. Signorelli	1	R04 (D. L. Love)	1
J. S. Fordyce		R30 (J. R. Dixon)	1
(Code MS 309-1)	1	R32 (R. A. Sutula)	1
H. J. Schwartz		R32 (W. A. Ferrando)	10
(Code MS 309-1)	1	R32 (Staff)	5
Cleveland, OH 44135		R32 (W. W. Lee)	1
		R33 (C. E. Mueller)	1

END

FILMED

1-85

DTIC